

## **Reservoir simulation and geomechanical modeling in Leming Lake, Alberta**

John J. Zhang, Tony Settari and Laurence R. Bentley

### **ABSTRACT**

This paper deals with reservoir simulation and geomechanical modeling. The physics of fluid flow and geomechanical systems is expressed as a set of conservation equations and simulation is their numerical solutions. GEOSIM is used to carry out simulation of a coupled reservoir and geomechanical model created using well logs, core measurements and seismic data. Reservoir simulation shows a spatial pattern of pressure, temperature and saturation changes around wells, which can be used to predict the change in seismic response. Geomechanical modeling shows significant displacements in the reservoir and in areas far away from the reservoir, but significant changes in stress and strain fields are mainly limited to the reservoir. Elastic moduli decrease due to exsolved gas released by lowering pressure and high temperature after a period of production. The moduli will be further reduced due to horizontal fractures predicted by geomechanical modeling. The cumulative effect is expected to be strong enough to be detected by time-lapse seismic data.

### **INTRODUCTION**

Heavy oil has been produced using cyclic steam stimulation from the Clearwater formation in Leming Lake, Alberta, Canada. Typically the process consists of scheduled cycles of injection and production from vertical, deviated or horizontal wells. High injection pressure is used to generate fractures, which sequentially introduces high temperature steam into the reservoir in hopes of improving injectivity and productivity. The steam chamber and temperature and pressure zones are conventionally forecasted with reservoir simulation. But the prediction is far from complete due to heterogeneity. Recently Imperial Oil shot time-lapse three-D seismic surveys over a few production pads in an attempt to monitor fluid flow and reservoir conditions. Seismic interpretations for changes in saturation, pressure and temperature in reservoirs add another constraint to reservoir simulation in addition to production history matching. Reservoir management based on reservoir simulation optimized by both production performance and time-lapse seismic would enhance heavy oil recovery. In this paper the authors focus on reservoir simulation and geomechanical modeling with an aim to evaluate how feasible time-lapse seismic can be in monitoring reservoir recovery.

### **UNDERLYING PRINCIPLES**

Fluid injection or/and production from a reservoir disturb the static equilibrium of pore fluids and solid framework. A natural tendency to reach a new balance initiates fluid flow and deformation. During the dynamic process conservation laws can be applied to affected. Equation (1) is the mathematical formula for fluid conservation (notation found at end of paper).

$$-\oint_s \rho_f \phi \mathbf{v}_f \cdot d\mathbf{s} = \frac{\partial}{\partial t} \left( \int_v \rho_f \phi dv \right) + Q_f, \quad (1)$$

where  $Q_f$  is the disturbance (amount of injected or produced fluid) leading to fluid pressure changes and fluid movement within the reservoir, which in turns causes changes of effective stress and deforms the solid framework. Similarly the conservation of grain solid mass is applicable, as shown in Equation (2):

$$-\oint_s \rho_s (1 - \phi) \mathbf{v}_s \cdot d\mathbf{s} = \frac{\partial}{\partial t} \left[ \int_v \rho_f (1 - \phi) dv \right] + Q_s. \quad (2)$$

The conservation of momentum for both fluid and grain solid are expressed in a vector form in Equation (3), which can also be derived from Newton's second law:

$$\oint_s \mathbf{S} \cdot d\mathbf{s} + \oint_s [\rho_s (1 - \phi) + \rho_f \phi] \mathbf{g} dv = \frac{\partial}{\partial t} \left\{ \int_v [\rho_s (1 - \phi) \mathbf{v}_s + \rho_f \phi \mathbf{v}_f] dv \right\}. \quad (3)$$

A secondary outcome of fluid flow and deformation is energy transfer in the media, which is expressed as an energy conservation Equation:

$$-\oint_s [\rho_f \phi \mathbf{v}_f H_f + \rho_s (1 - \phi) \mathbf{v}_s H_s + C_T \nabla T] \cdot d\mathbf{s} = \frac{\partial}{\partial t} \left\{ \int_v [\rho_f U_f \phi + \rho_s U_s (1 - \phi)] dv \right\} + Q_{\text{heat}} \quad (4)$$

Applying the Green-Gauss theorem and removing the integral over the representative volume  $v$ , we obtain the following equations:

$$-\nabla \cdot (\rho_f \phi \mathbf{v}_f) = \frac{\partial}{\partial t} (\rho_f \phi) + Q_f, \quad (5)$$

$$-\nabla \cdot [\rho_s (1 - \phi) \mathbf{v}_s] = \frac{\partial}{\partial t} [\rho_f (1 - \phi)] + Q_s, \quad (6)$$

$$\nabla \cdot \mathbf{S} + [(1 - \phi) \rho_s + \phi \rho_f] \mathbf{g} = \frac{\partial}{\partial t} [\rho_s (1 - \phi) \mathbf{v}_s + \rho_f \phi \mathbf{v}_f], \quad (7)$$

and

$$-\nabla \cdot [\rho_f \phi \mathbf{v}_f H_f + \rho_s (1 - \phi) \mathbf{v}_s H_s + C_T \nabla T] = \frac{\partial}{\partial t} [\rho_f U_f \phi + \rho_s U_s (1 - \phi)] + Q_{\text{heat}}. \quad (8)$$

The fluid velocity is related to Darcy velocity,  $\mathbf{v} = (\mathbf{v}_f - \mathbf{v}_s) \phi$ , and Equation (5) for single-phase fluid flow can be reformulated as:

$$-\nabla \cdot [\rho_f k / \mu_f (\nabla P - \rho_f \mathbf{g}) + \rho_f \phi \mathbf{v}_s] = \frac{\partial}{\partial t} (\rho_f \phi) + Q_f. \quad (9)$$

For a multi-component, multi-phase system, the equation is decomposed into a number of equations that correspond to each component.

Considering that the time scales in days during hydrocarbon recovery is very large compared with the magnitude of displacements in millimeters or smaller,  $\mathbf{v}_s$  is negligibly small. Consequently, all the terms multiplied by  $\mathbf{v}_s$  can be eliminated. Likewise Equation (6) is insignificant and can be removed from the group of equations. In addition,  $\mathbf{v}_f$  is typically around 10 m/day and  $\partial \mathbf{v}_f / \partial t$  is much smaller. To the first-order approximation, the term related to  $\mathbf{v}_f$  on the right-hand side in Equation (7) can be omitted. A final set of equations result as follows:

$$-\nabla \cdot [\rho_f k / \mu_f (\nabla P - \rho_f \mathbf{g})] = \frac{\partial}{\partial t} (\rho_f \phi) + Q_f, \quad (10)$$

$$-\nabla \cdot [\rho_f k / \mu_f \nabla P H_f + C_T \nabla T] = \frac{\partial}{\partial t} [\rho_f U_f \phi + \rho_s U_s (1 - \phi)] + Q_{\text{heat}}, \quad (11)$$

and

$$\nabla \cdot \mathbf{S} + [\rho_s (1 - \phi) + \rho_f \phi] \mathbf{g} = 0. \quad (12)$$

Total stress  $\mathbf{S}$  is resolved into the sum of fluid pressure and effective stress, which relates to the displacements through the constitutive equation. As a result, Equation (12) has two unknowns (pressure and displacement vector). All together, Equations (10), (11) and (12) have three unknowns and the solution is unique.

A numerical solution to Equations (10) and (11) is traditionally called reservoir simulation, which finds fluid pressure, temperature and saturations (if it is a multi-phase flow). There are many commercial software packages for this purpose such as STARTS, EXOTHERM, TETRED, ECLIPSE, VIP, GEOSIM etc., which can handle multi-phase multi-component fluid flow and heat transfer.

A limitation of traditional reservoir simulation is that porosity and permeability are assumed to be constant or are artificially set as a function of fluid pressure. For well consolidated rocks, this treatment may not generate substantial errors. For unconsolidated sands, however, deformation is significant especially when fractures are generated. Porosity and permeability evolution during injection and recovery need to be accurately calculated in order to have accurate reservoir simulations. On the other hand, the stress field disturbed by production and/or injection is not limited to the reservoir and the surrounding area may undergo significant stress changes and deformation. The uplift in Cold Lake after steam injection appears to result from considerable thermal expansion far beyond the production zone. The geomechanical modeling therefore must be coupled with traditional reservoir simulation.

Reservoir simulation and geomechanical modeling can be fully coupled, i.e., Equations (10), (11) and (12) solved simultaneously, but we rarely do that. Reservoir simulation and geomechanical modeling have been developed separately in the last decades. The commonly used solution method is iteration or partial coupling between the two independent applications. If iterated to full convergence, it solves the problem as rigorously as a fully coupled (simultaneous) solution (Settari, 1998). The link is fluid pressure and porosity and permeability. The pressure computed from reservoir simulation

in a time step passes as an input to geomemechanical modeling, which computes displacements, strains and stresses. The new porosity and permeability computed from strains are then used by the reservoir simulator, which re-computes the pressure and other unknowns. This process is repeated until convergence.

### RESERVOIR CHARACTERIZATION MODEL

The reservoir characterization model defines the geometry and physical properties of the reservoir, which are the input for the reservoir simulation. In the companion paper, the authors describe a reservoir characterization model developed from core measurements, well logs and three-dimensional seismic data. This section discusses boundary conditions, gridding and how to scale up the physical properties from the small scale for seismic data to the coarser grid used for reservoir simulation.

As shown in Figure 1, 3-D seismic surveys were repeated in March 1997, February 1998 and February 1999 in an attempt to monitor the five horizontal wells for cyclic steam stimulation and production. Steam injection started in September 1997 and the 1997 seismic survey is then viewed as the baseline for these five horizontal wells. The adjacent deviated wells in the survey area were also injected and produced at the same period and at much earlier times as well. Although they affect the 3-D survey area, their interaction is neglected for the moment and will be detailed later in the future study. Since the simulator boundaries are no-flow boundary, the area for reservoir simulation was extended on three sides beyond the seismic survey area, as shown in Figure 1.

The three-dimensional seismic surveys cover an area of 1200 m \* 960 m with 120\*96 stacked traces. The bin size is 10 m \* 10 m. The reservoir zone extends vertically for 50 m from 410 ms to 460 ms, sampled at an interval of 1 ms. If this grid was for reservoir simulation, the total number of blocks exceeds half a million. A coarser grid is required in order to carry out the task of reservoir simulation. By experiment, a grid of 40\*36\*20 was finally selected for the area with seismic data and then an additional grid beyond that was three by four cells, as seen in Figure 2. This is a tradeoff between horizontal and vertical resolution.

Horizontally, each reservoir simulation cell contains six seismic traces. Vertically, 50 time samples correspond to 20 cells and averaging can not be achieved for each cell. It is noted from the companion paper that the most important thing from the seismic section is locations of peaks, which are attributed to the existence of tight rocks with zero porosity and zero permeability. Well logs and core measurements indicate that the thickness of tight rocks is approximately 2 meters. We re-sampled the time window of 50 ms at an interval of 0.5 ms. The new total number of samples is 100 and each sample represents 0.6 meter. Each assumed tight rock peak and the two immediately adjacent samples are assumed to be tight rock. So each peak corresponds to 1.8 meters of tight rock.

Now each reservoir simulation cell contains 3\*3\*5 seismic sub-cells. Averaging can be done to find its porosity and permeability. The porosity is simply an arithmetic average of 45 seismic sub-cells. Permeability, however, is more complicated. We assumed that oil sands have a horizontal and vertical permeability of 2000 md and 650 md, respectively. The permeability for tight rocks is zero. The averaging methodology is

as follows: averaging first along z direction for each of nine vertical columns of sub-cells, arithmetic for  $K_x$  and  $K_y$  and harmonic for  $K_z$ . Second along y direction for each of three rows, arithmetic for  $K_x$  and  $K_z$  and harmonic for  $K_y$ . Finally along x direction to average the last remaining sub-cells, harmonic for  $K_x$  and arithmetic for  $K_y$  and  $K_z$ . The final result is as shown in Figure 3 and 4.

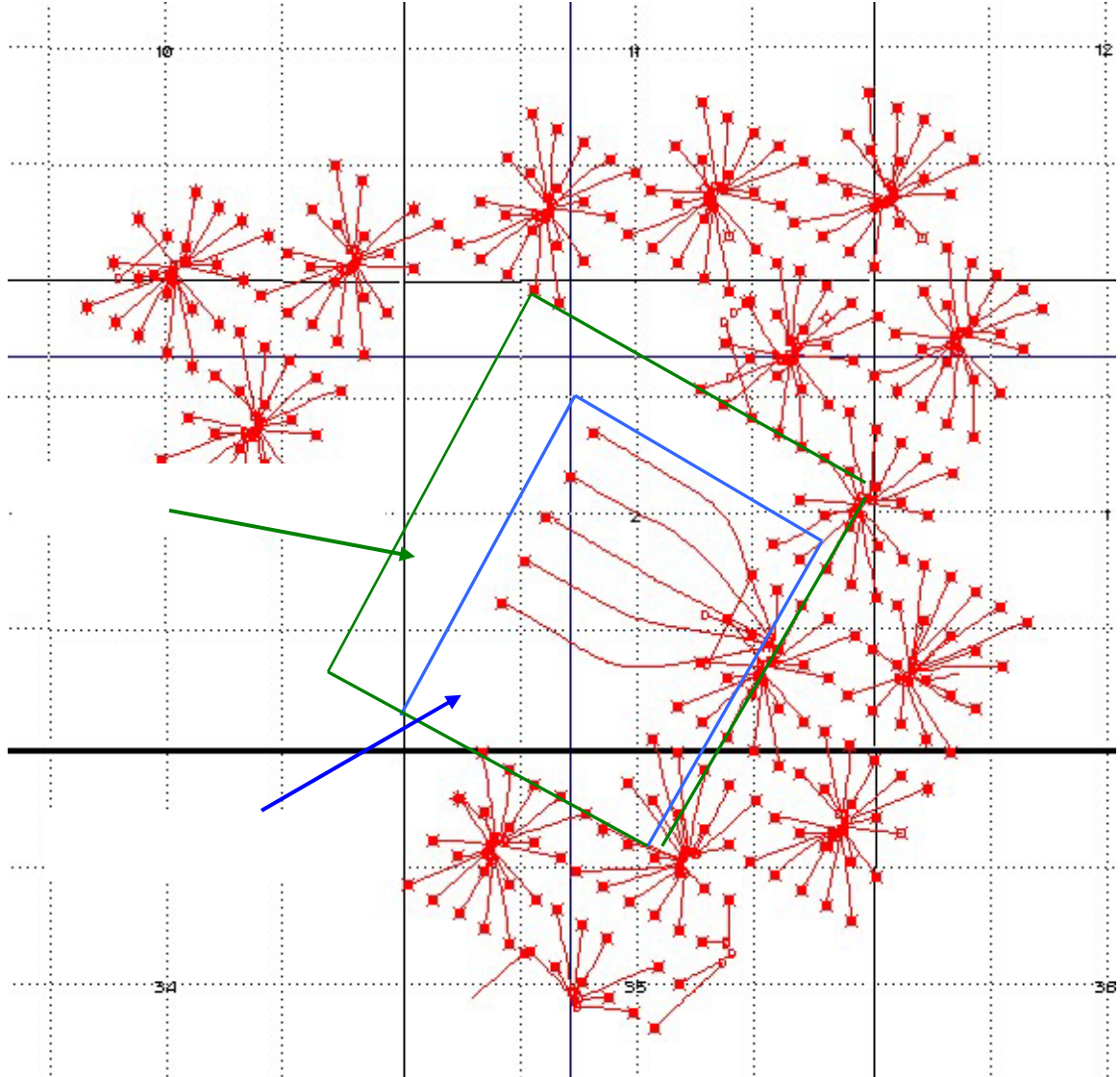


FIG. 1 Time-lapse 3-D seismic survey area (blue) and reservoir simulation area. The goal of time-lapse seismic surveys was to monitor the five horizontal wells for cyclic steam stimulation.

### GEOMECHANICAL MODEL

One of the goals of geomechanical modeling is to find changes in stress and strain far beyond wells and the reservoir. The geomechanical model is set to include the reservoir and surrounding formations. Restricted by computer memory and speed, the number of blocks outside of the reservoir must be limited. As seen in Figure 5, we chose a number of important seismic reflections above the reservoir as block boundaries and extended the

model to the surface. The blocks below the reservoir extend downward over one thousand meters. The horizontal boundary defined in reservoir simulation is applied to geomechanical modeling and it is defined as a no-displacement boundary condition. The whole grid for geomechanical model is seen in Figure 6.

The static moduli for geomechanical modeling are often acquired from extensive lab testing and modeling, which are limited to a few samples from target zones. Despite their validity at coring locations, a large area is left without data and interpolation and extrapolation from a few points is not reliable. On the other hand, well logs and seismic data are abundant and dynamic moduli can be calculated from them and used to populate the whole area. The key is how to convert dynamic moduli, which measure stress-strain relationship at low strain amplitude and at a short period of time, to static moduli, which describe full long-term stress-strain. The dynamic and static moduli are different because materials are elastic for the former and undergo partially irrecoverable deformation for the latter. In this study, we blocked sonic and density logs according to the vertical grid of the geomechanical model and computed the dynamic moduli. An empirical relationship between dynamic Young's modulus and static Young's modulus was applied to calculate the static moduli. The equation is  $E_s = a E_d^b$  ( $a=0.097$  and  $b=1.485$ , Wang and Nur, 2000).  $E_s$  is static Young's modulus and  $E_d$  is dynamic Young's modulus. Most values were found to be close to those obtained from lab testing (Walters and Settari, 2002).

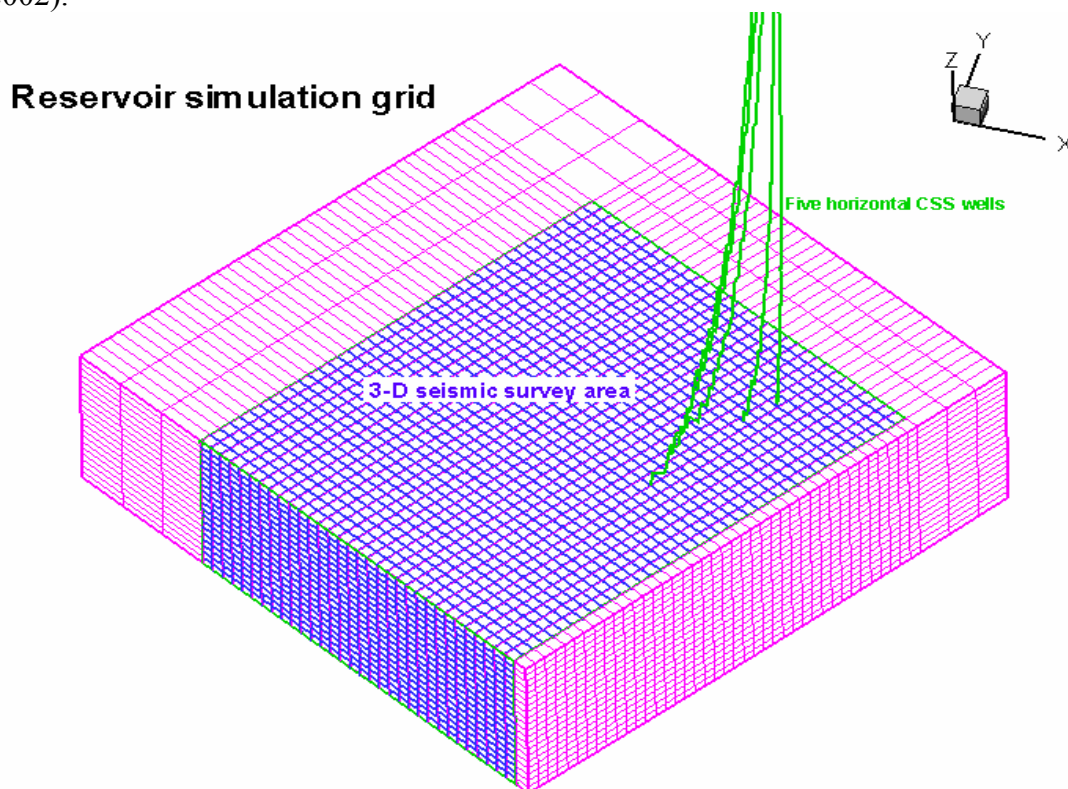


FIG. 2. Three-dimensional visualization of reservoir simulation grid (43\*36\*20). The seismic survey area has a dimension of 40\*36.

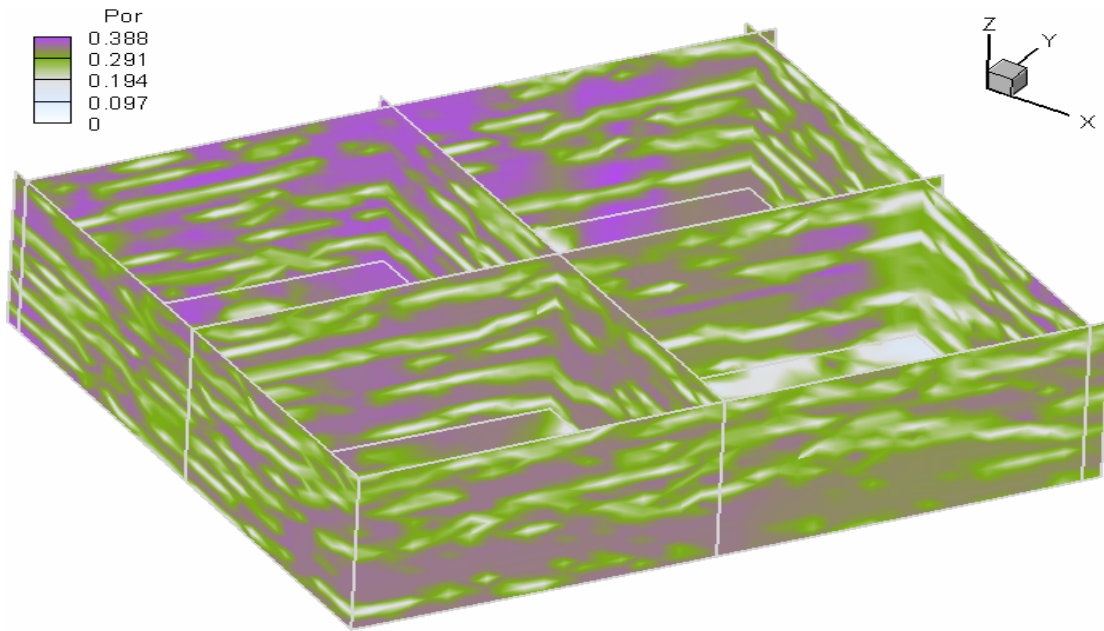


FIG. 3. Three-dimensional visualization of porosity in the area with seismic data

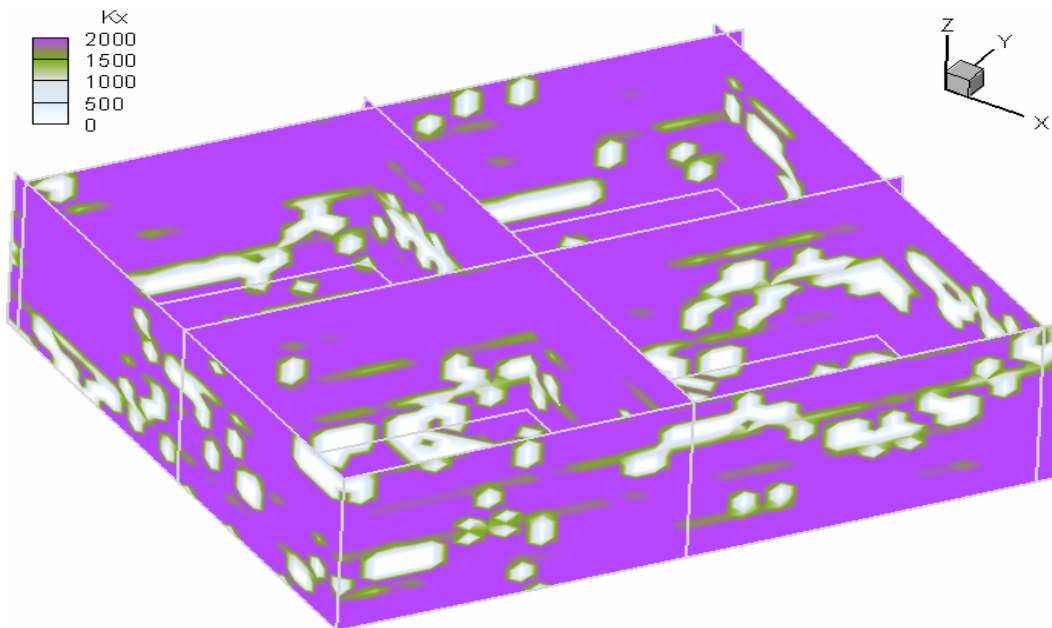


FIG. 4. Three-dimensional visualization of permeability (horizontal) in the area with seismic survey

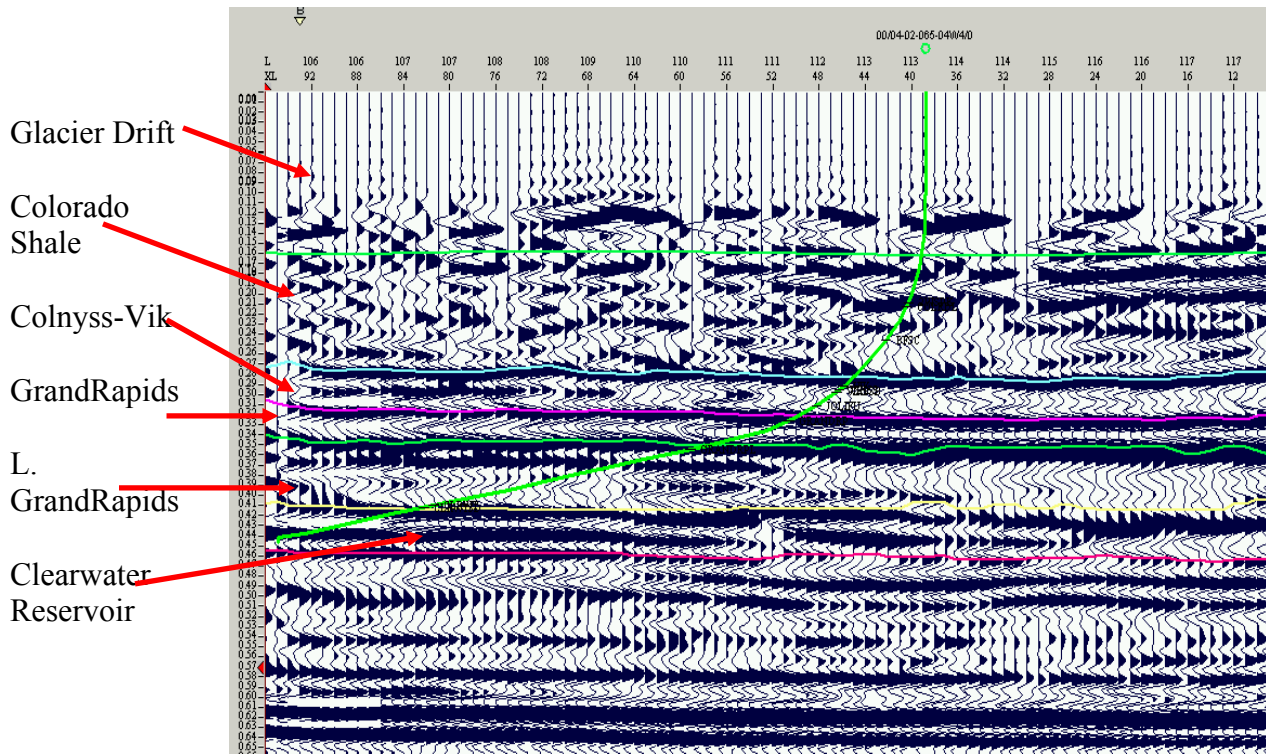


FIG. 5. Seismic section in the north-south direction. It shows the major strata above the reservoir.

**Geomechanical modeling grid**

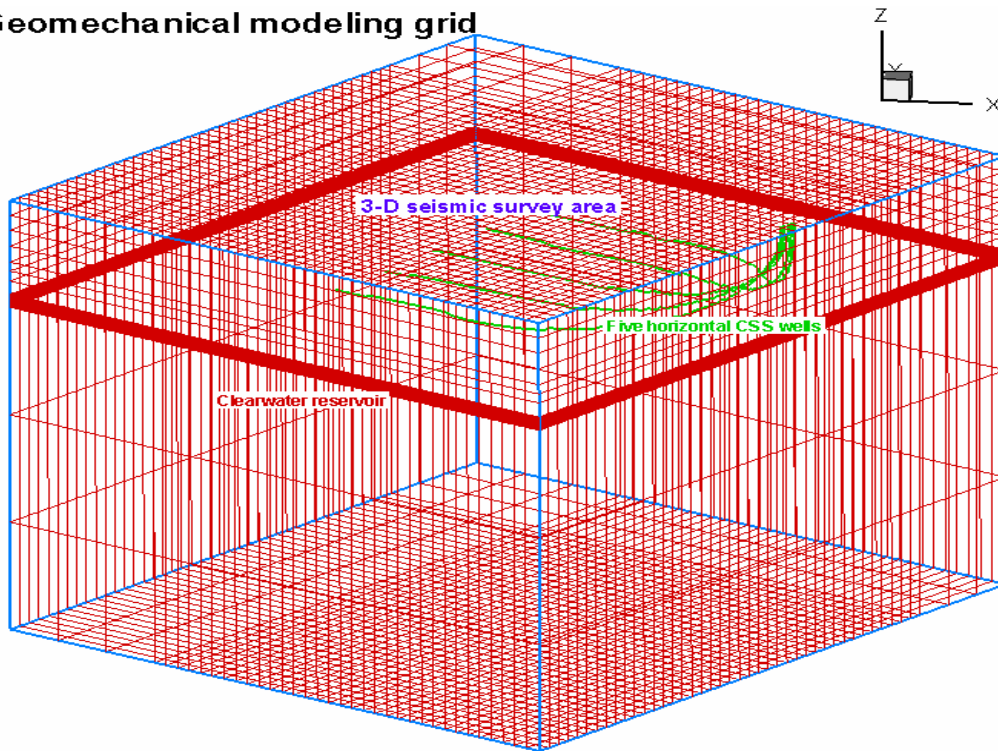


FIG. 6. Three-dimensional visualization of geomechanical modeling (43\*36\*30). The seismic survey area has a dimension of 40\*36.

## SIMULATION PARAMETERS

In addition to porosity, permeability and static moduli, many other parameters are needed to be defined. We used the mode of light oil to simulate cyclic steam injection into the Clearwater formation in Leming lake. The mode is a three-component and three-phase formulation. The three components are water, light oil and heavy oil and the three phases are water, gas and oil. Depending on pressure and temperature, light oil could be in gas phase or in oil phase or in both. Similarly water was allowed to exist in both gas phase and water phase. But heavy oil is not allowed to vaporize. The three-phase relative permeability was computed from two relative permeability tables for a water-oil system and a liquid-gas system using a modification of Stone's II equation (Walters and Settari, 2000). Other rock physical properties were provided by Taurus Reservoir Solution.

Settari and Raisbeck (1978) measured the vertical and horizontal stresses at a number of depths in poorly consolidated sands in Cold Lake. They found the vertical stress gradient was 21.3 kPa/m and the horizontal stress gradient was 20.0 kPa/m. The number was used as input for simulation. The initial distribution of stress implies that vertical fractures would be opened if steam was injected. However, the horizontal fractures were created when steam was injected because steam injection changed the stress field.

## SOFTWARE TOOL

The coupled reservoir simulation-geomechanical modeling was performed with GEOSIM, a software package by Taurus Reservoir Solution. GEOSIM is a modular software system combining a 3-D, 3-phase thermal reservoir simulation with a general 3-D finite element stress-strain simulation (Walters and Settari, 2000). TERASIM-THERM models the flow of oil, steam, water and non condensing (NC) gas in an oil reservoir with heat transfer in the reservoir and over/under-burden. Steam injection and production can be modeled under thermal conditions. FEM3D analyses coupled poro- and thermoelasticity for stresses and deformations. As mentioned previously, the two components are partially coupled or iterated until convergence.

## RESULTS AND DISCUSSION

The time-lapse seismic surveys were conducted to monitor the steam chamber and the distribution of pressure, temperature and saturation for five horizontal wells. The influence from other adjacent wells probably needs to be accounted for, but they have been neglected for the time being.

Steam injection started in September, 1997, for three of the western horizontal wells. It lasted for two months to October for two wells and was followed by production in November. The third well was injected for three months to November, and began to produce in January 1998. The other two wells on the east side were injected in October until November and production started in January 1998. In February 1998, when first time-lapse seismic survey was done, all wells were on production. Our simulation started from September at the beginning of injection and continued to the end of February, 1998.

Figure 7 shows the 3-D visualization of oil saturation after thirty-eight-day injection for three wells. The saturation decrease is immediately around the injection wells and this

zone could be viewed as the steam chamber. Away from the wells, the saturation goes back to normal quickly and it appears that the effect is limited to around 30 meters. The zone of high temperature, as seen in Figure 8, is larger than the steam chamber, spanning three cells around 100 metres. The temperature anomaly is also observable above the well in the middle. As indicated in Figure 9, fluid pressure propagates faster than temperature and saturation changes and forms a unified high-pressure regime, which may be useful in generating fractures conducive to fluid flow and heat transfer. The scope of influence from fluid pressure exceeds 200 meters. These three pictures show that three zones are formed: steam chamber, temperature anomaly and fluid pressure front. These three zones would have different velocities and densities and would respond differently seismically.

In October, the other two wells were first injected and injection continued to November. The two wells on the west side started production in November after two-month injection. The remaining well in the middle was injected until November. The following three pictures show conditions at the end of November. In Figure 10, the oil saturation around two wells on the west side decreases because of production. Two steam chambers can be found for two wells on the east side. In Figure 11, the temperature zone for two wells on the west side has expanded even though they are on production. The temperature zone increases for the well in the middle due to continued injection. In Figure 12, the fluid pressure drops for the two wells on the west side. Once again, fluid pressure is the most rapidly propagating parameter and it declines promptly with production. If the velocity is affected by fluid pressure significantly because of gas dissolution or ex-solution, the front can be captured by seismic signals.

In February 1998, the first time-lapse seismic survey was shot in an attempt to capture changes in reservoir conditions. At this time, all wells are already on production for two months and we expect pressure decline. Temperature may not change much and oil saturation around the boreholes may increase compared to steam injection periods as heated oil flows into the. In Figure 13, oil saturation does increase slightly around all the wells. In Figure 14, temperature decreases a little. In Figure 15, the high pressure zone shrinks and low pressure zones expand away from wells. Time-lapse seismic response in the region around wells may be strong since high temperature and exsolved gas will decrease the bulk modulus, however low fluid pressure will increase frame dry modulus.

Geomechanical modeling serves two purposes, as mentioned previously. One is to couple with reservoir simulation for more accurate results, which has been done in the foregoing part. The other is to find stress, strain and displacements in areas far beyond the reservoir zone. They may cause collective seismic responses larger than those due directly to changes within the reservoir. Kenter etc. (2004) found that time shift in overburden formations due to hydrocarbon recovery can be an order of magnitude larger than changes found in the reservoir. In the following, we will show a few pictures and examine how these geomechanical parameters respond to steam injection and production in the reservoir zone.

On thirty-eighth day after injection in the three wells on the west side, the vertical stress does not change appreciably in most of the overburden formations as shown in Figure 16, but it becomes negative within the reservoir, a substantial deviation from initial stress. Note that  $S_z$  is effective stress, which indicates horizontal fractures are

generated by steam injection. Horizontal stresses have a similar distribution. No stress change implies that seismic data may not be able to detect steam injection from overburden formations as Kenter suggested (2004). Figure 17 exhibits volumetric strain, which is limited to the reservoir zone and has little influence on the overburden formation as expected from stress. However, the vertical displacement is significant and in excess of a few millimeters on ground in Figure 18. Relatively large displacements accompanied by insignificant stress is attributed to small moduli in unconsolidated sands and shale in overburden formations.

At the end of November 1997 (seventy-sixth day), the two wells on the east side have been injected for two months. Injection in the well in the middle has continued for three months. The two wells on the west side are on production. In Figure 19, the high magnitude of negative vertical stresses are situated in the newly injected wells, while they have become relatively small, even positive, in two wells put on production in November. Different from the scenario in Figure 17, the volumetric strain has reached the ground surface as seen in Figure 20. This is caused by prolonged injection in the underlying reservoir. The expansion of the overlying formation may decrease the elastic moduli and may be seismically detectable. The vertical displacements of the overburden are further increased and expanded to a larger area as shown in Figure 21. The uplift at the ground surface is on the order of centimetres.

In February 1998, all wells were on production. It is expected that vertical stress decreases and could be positive within the reservoir, depending on the duration and quantities of oil production. The volumetric strain is expected to drop and become negative. The vertical displacements should decrease. Figure 22 indicates an increase in vertical stresses in the reservoir zone compared to injection times. As a matter of fact, vertical stresses have become positive, which may cause fractures created during steam injection to close. In Figure 23, the volumetric strain remains positive and the initial state has not been restored. In Figure 24, the vertical displacements still maintain high values. The implication is that the horizontal fractures existed at the time of the first time-lapse seismic survey and we expect low frame moduli. Combined with the previously mentioned fluid factors, the elastic moduli in the reservoir zone is expected to be much lower than the initial moduli. We expect it is feasible to monitor these zones seismically. The changes of elastic moduli in the overburden appear not to result in substantial time shift and it may not be feasible to see the changes seismically.

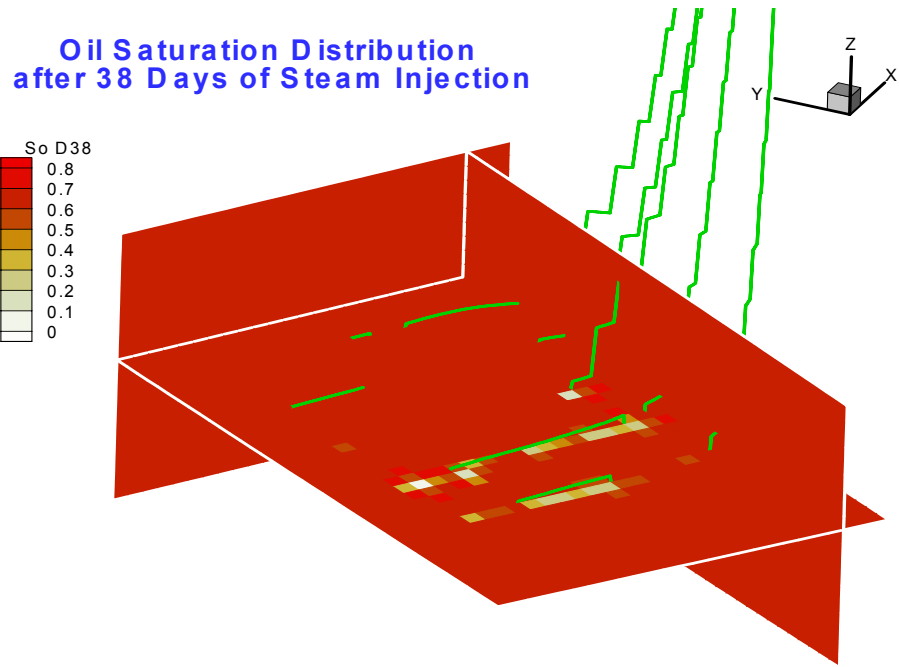


FIG. 7. Distribution of oil saturation after one-month steam injection.

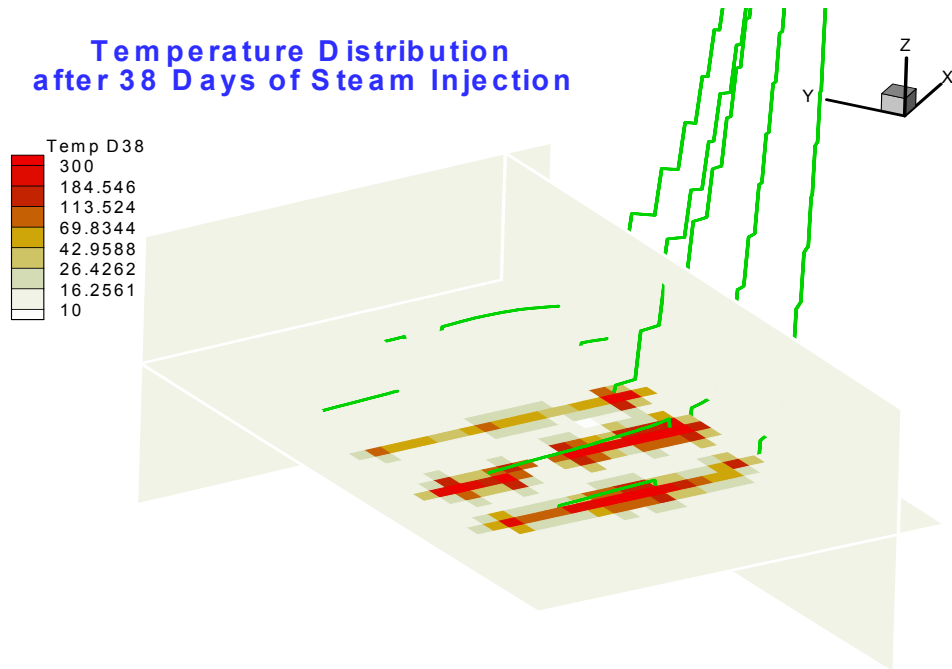


FIG. 8. Distribution of temperature after one-month steam injection.

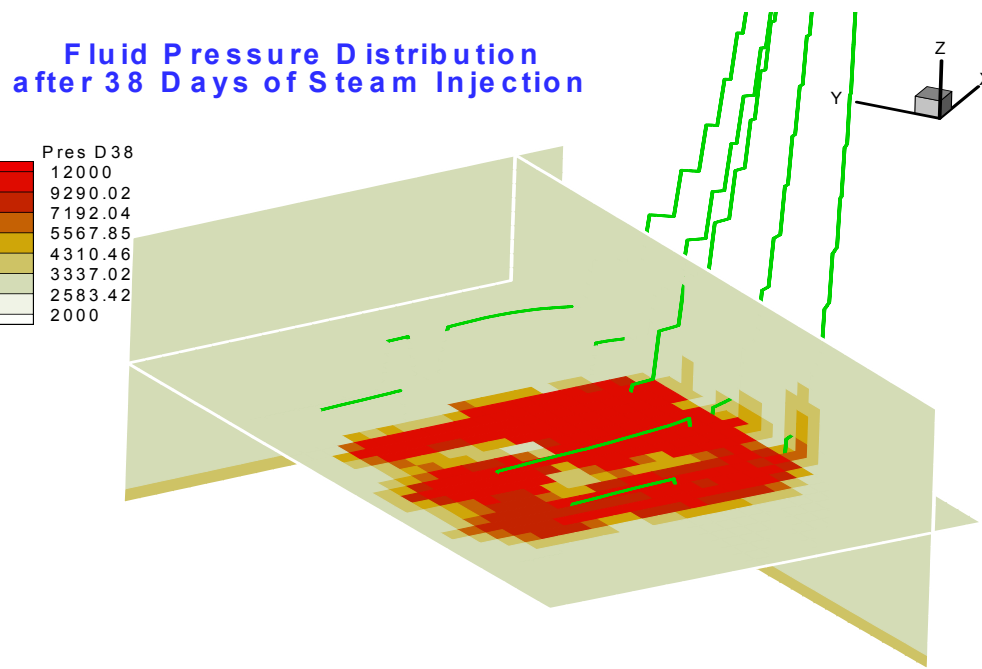


FIG. 9. Distribution of fluid pressure after one-month steam injection.

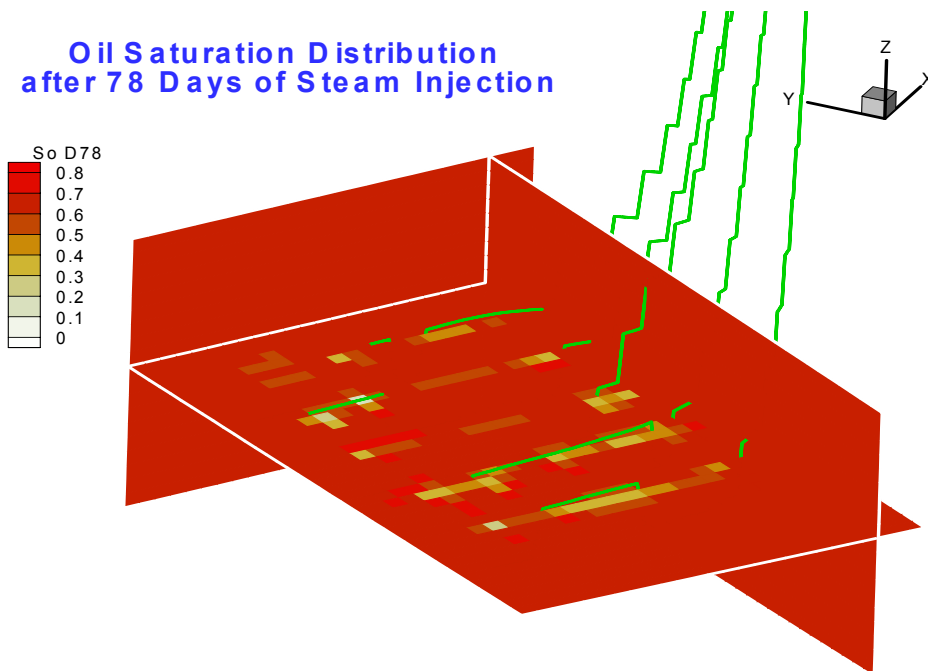


FIG. 10. Distribution of oil saturation after more than two-month steam injection.

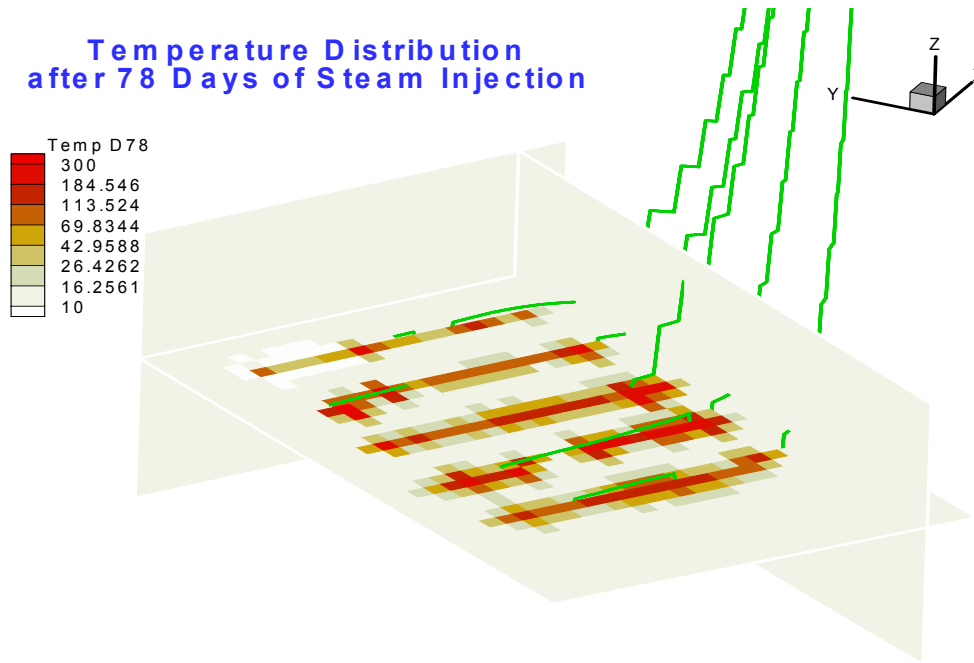


FIG. 11. Distribution of temperature after more than two-month steam injection.

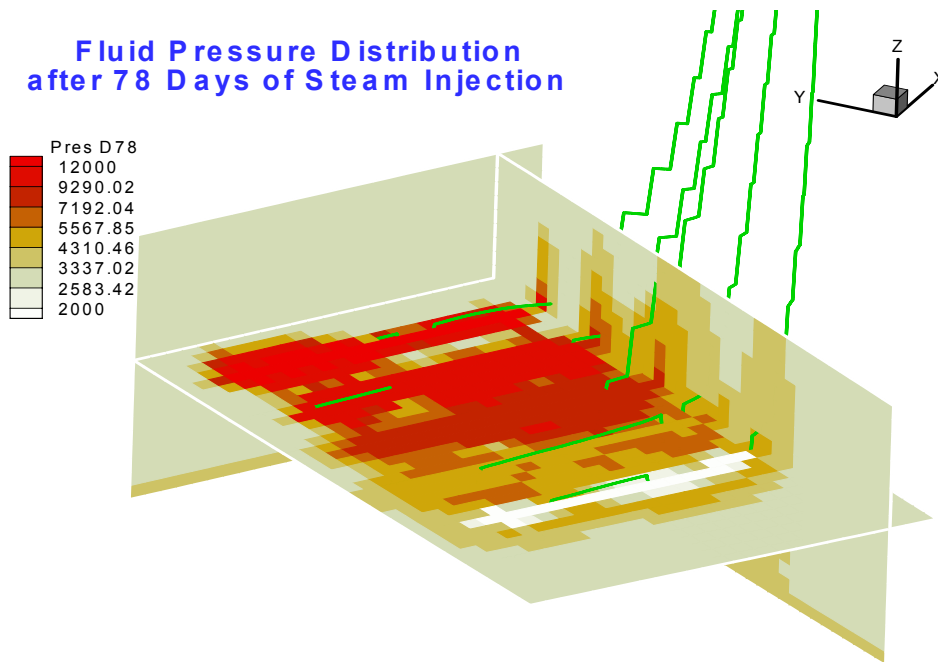


FIG. 12. Distribution of fluid pressure after more than two-month steam injection.

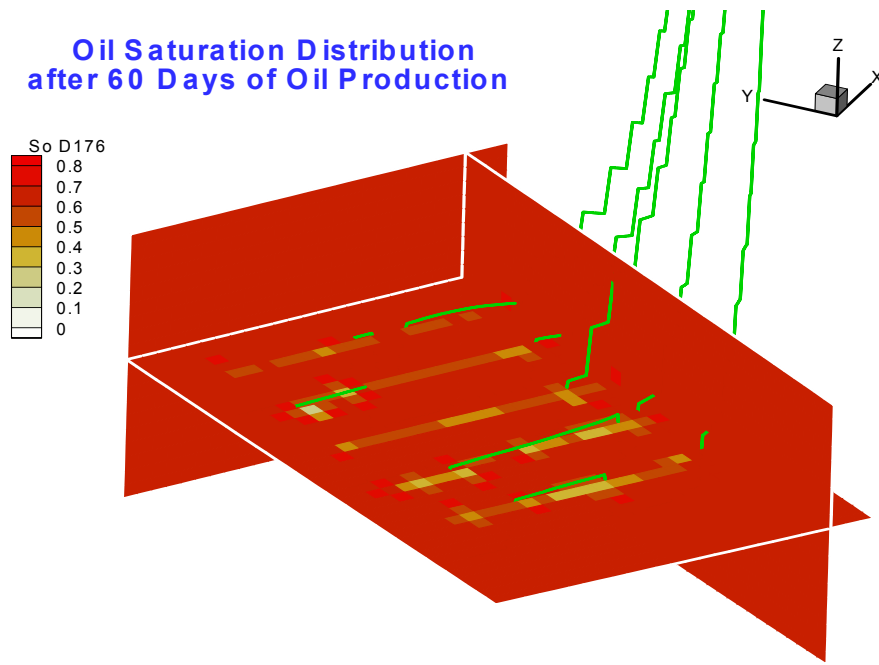


FIG. 13. Distribution of oil saturation after two-month oil production.

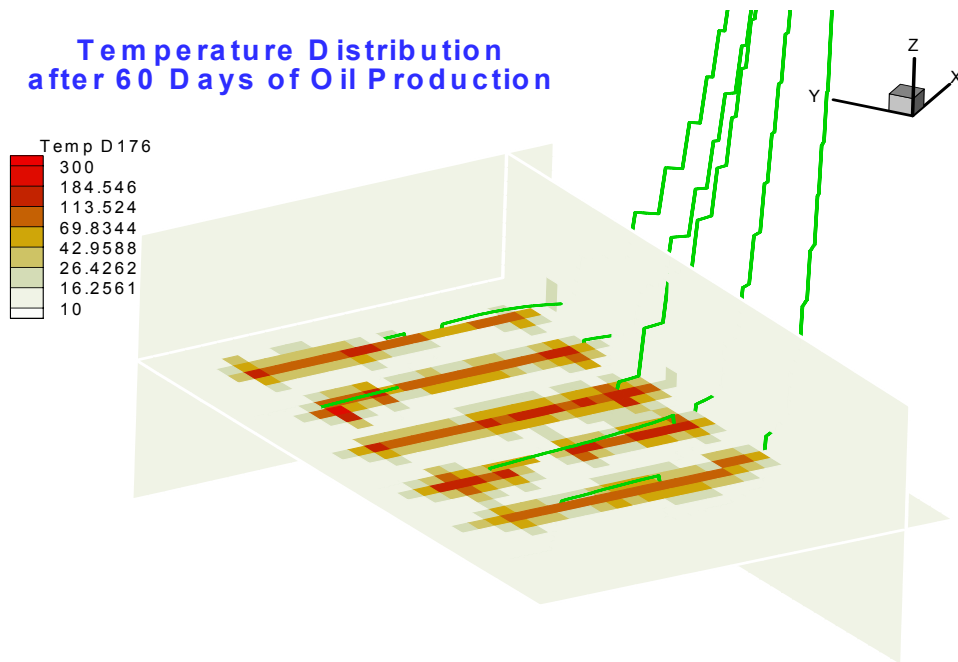


FIG. 14. Distribution of temperature after two-month oil production.

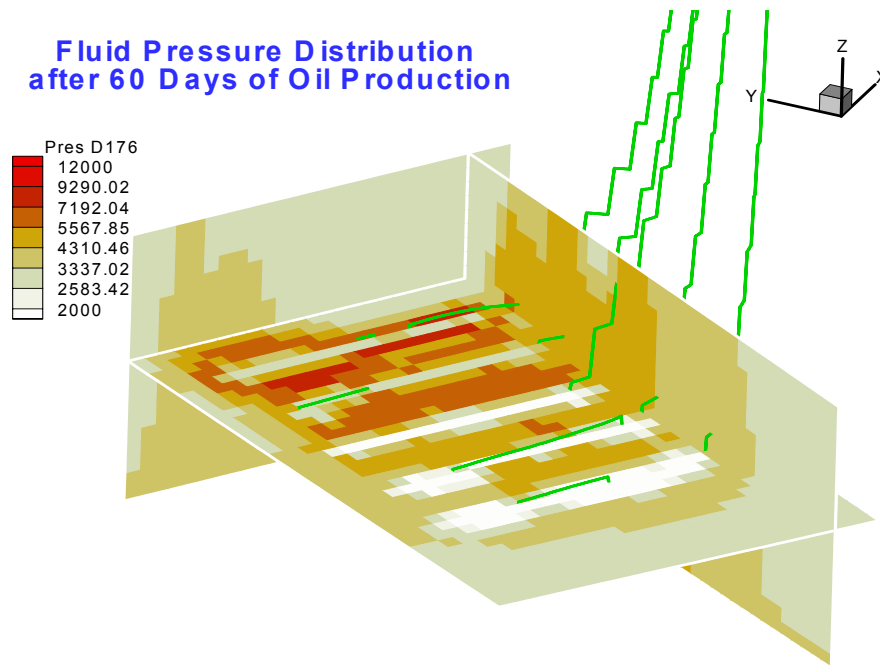


FIG. 15. Distribution of fluid pressure after two-month oil production.

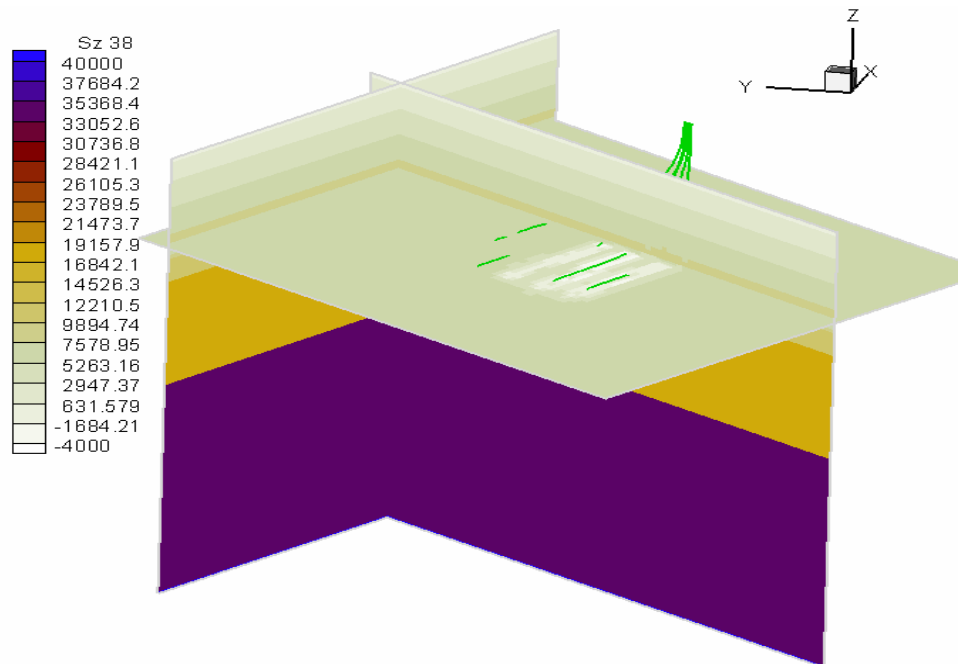


FIG. 16. Distribution of vertical stresses in the reservoir and overburden formations on thirty-eighth day after injection (the unit is in KPa).

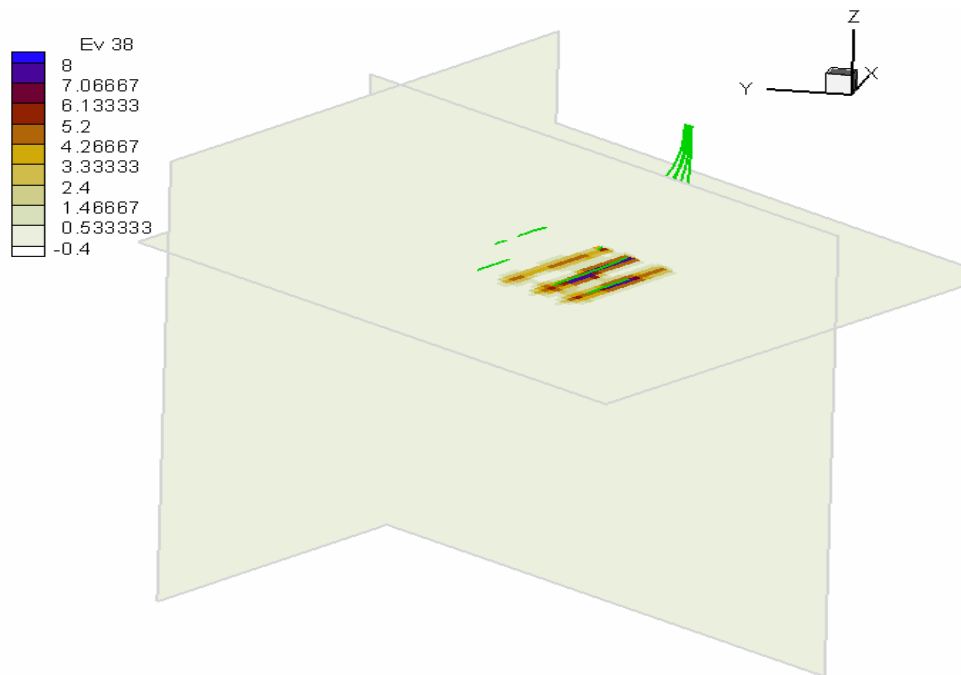


FIG. 17. Distribution of volumetric strains in the reservoir and overburden formations on thirty-eighth day after injection (the unit is in %).

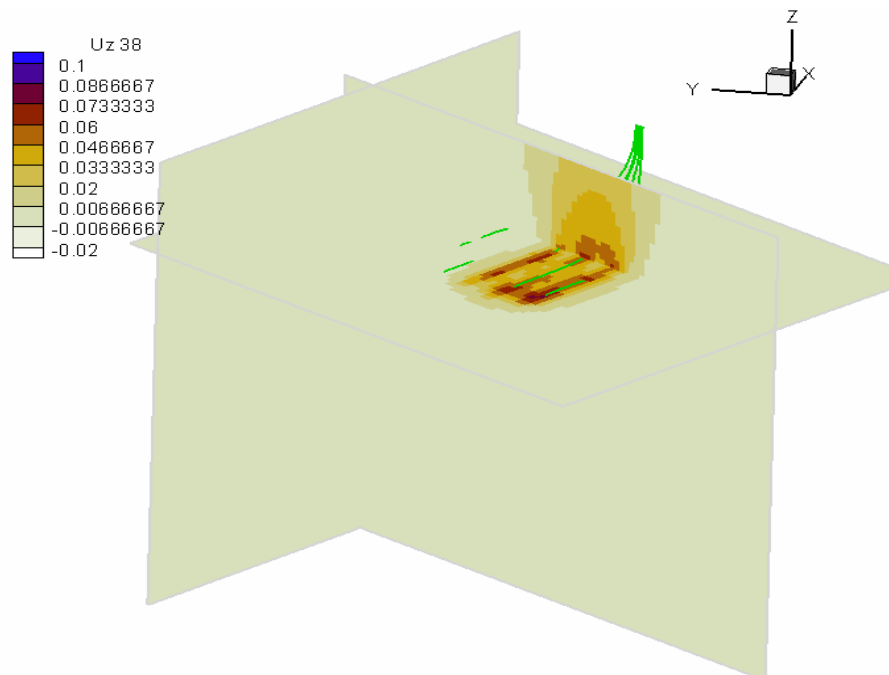


FIG. 18. Distribution of vertical displacements in the reservoir and overburden formations on thirty-eighth day after injection (the unit is in meter).

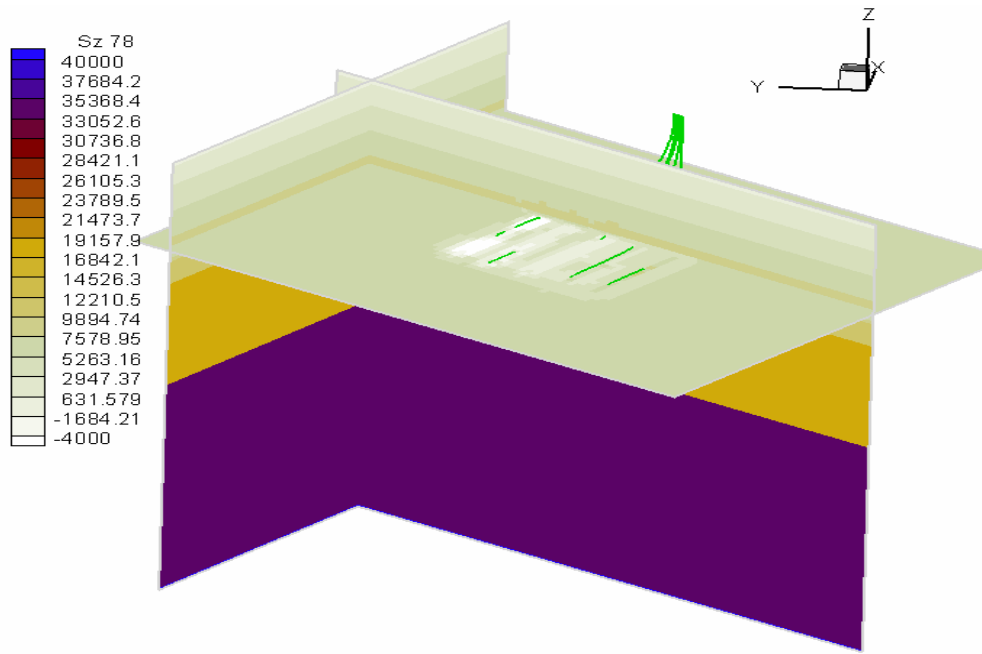


FIG. 19. Distribution of vertical stresses in the reservoir and overburden formations on seventy-eighth day after injection (the unit is in KPa).

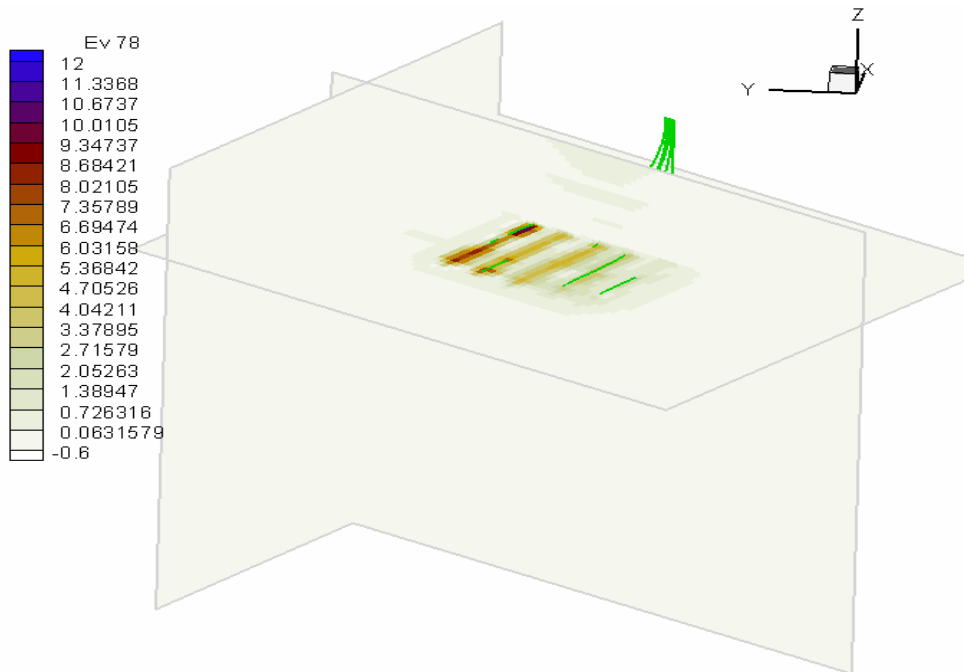


FIG. 20. Distribution of volumetric strains in the reservoir and overburden formations on seventy-eighth day after injection (the unit is in %).

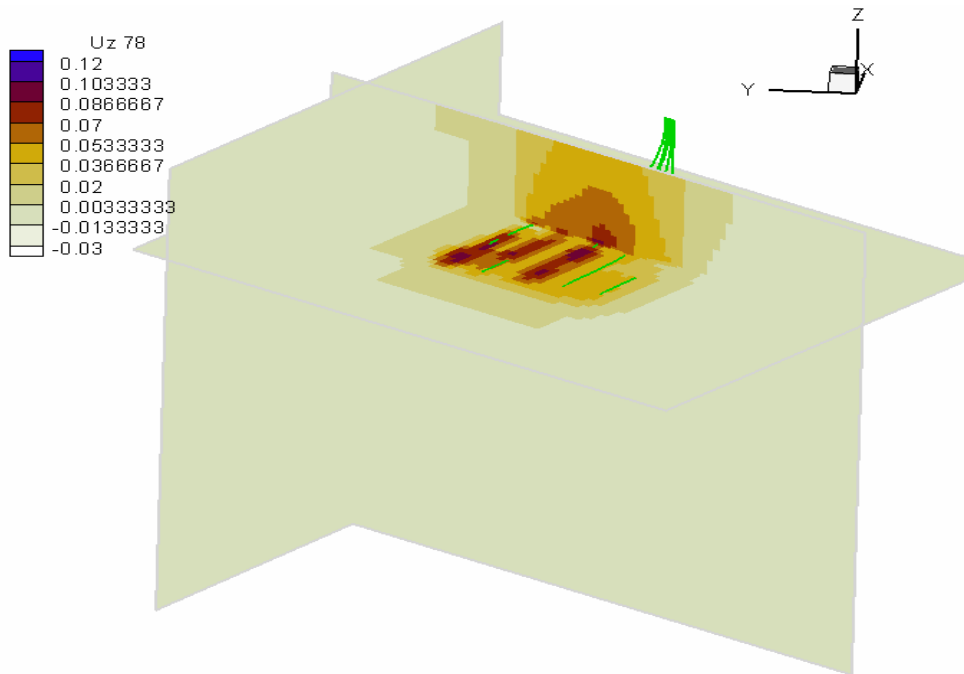


FIG. 21. Distribution of vertical displacements in the reservoir and overburden formations on seventy-eighth day after injection (the unit is in meter).

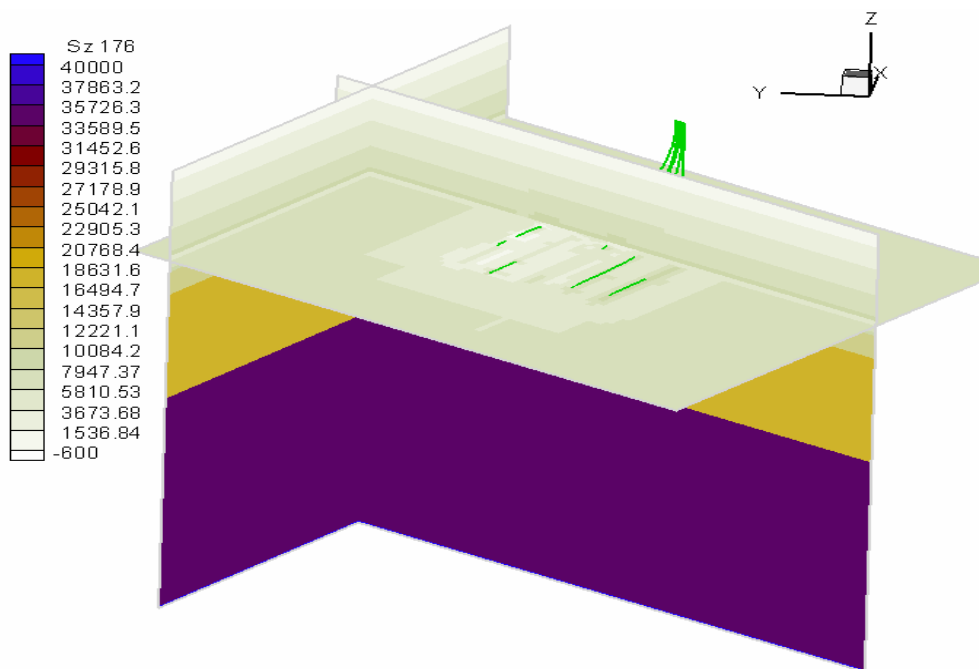


FIG. 22. Distribution of vertical stresses in the reservoir and overburden formations after two-month production (the unit is in KPa).

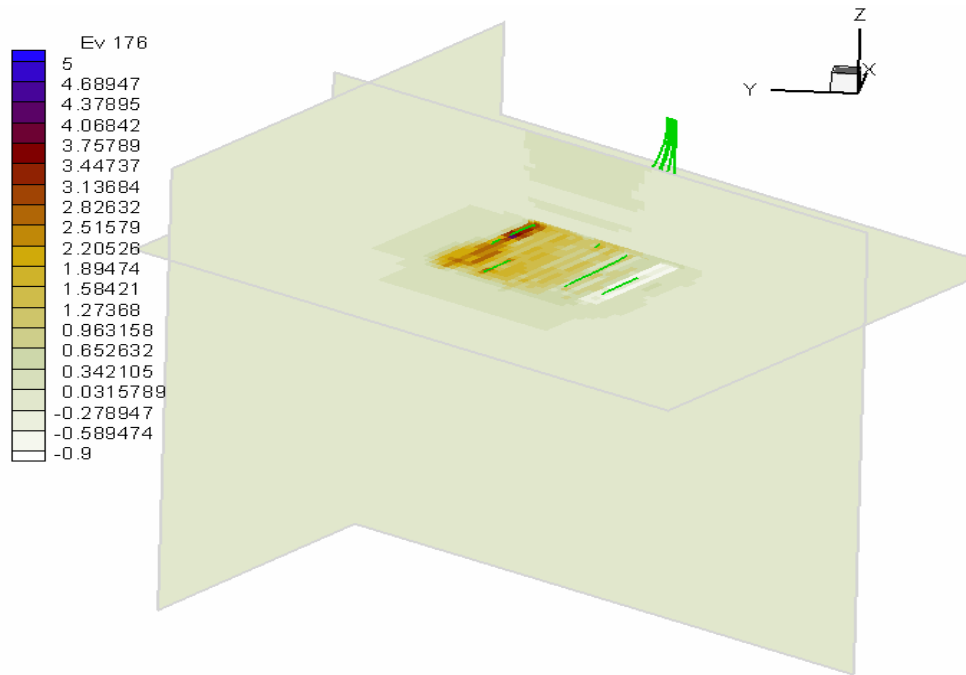


FIG. 23. Distribution of volumetric strains in the reservoir and overburden formations after two-month production (the unit is in %).

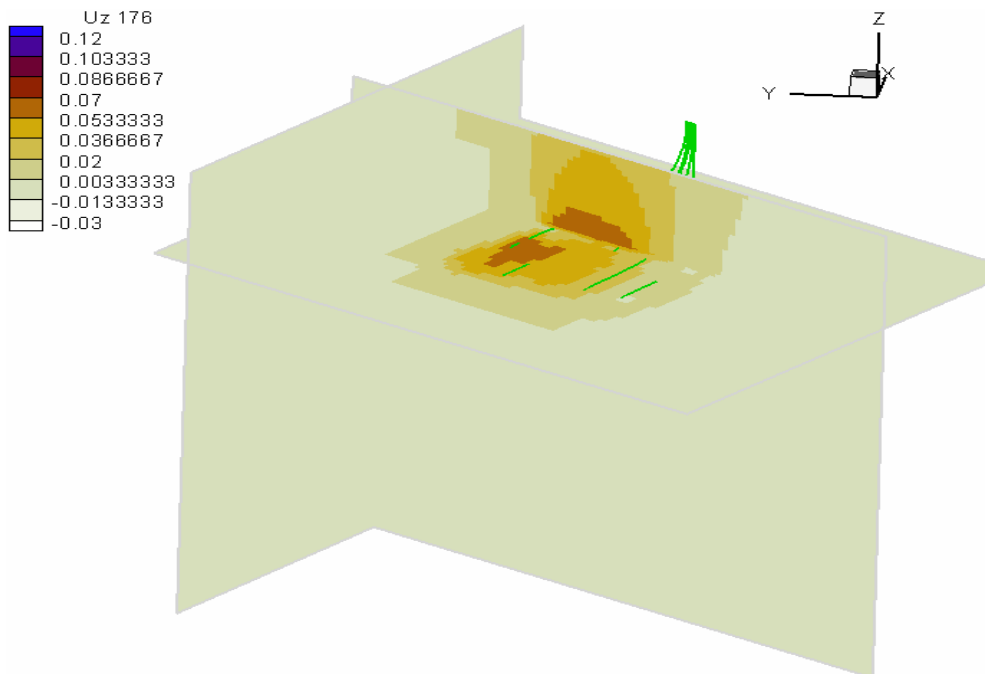


FIG. 24. Distribution of vertical displacements in the reservoir and overburden formations after two-month production (the unit is in meter).

## CONCLUSIONS

The principle of coupling reservoir simulation with geomechanical modeling is to solve the equations of conservation (mass, energy and momentum) by iteration between flow simulations and geomechanical simulations. A reservoir characterization model suitable for reservoir and geomechanical simulation was created for a portion of the Leming Lake reservoir.

Reservoir simulation shows zones of changing saturation, pressure and temperature around injection wells. Reservoir simulation shows the after a period of production low pressure exsolves gas from the oil. The gas plus the high temperature contribute to lowering the bulk moduli. However, the lower pressure will cause an increase in effective stress tending to increase the dry frame moduli.

Geomechanical modeling reveals stress, strain and displacements in the reservoir and in areas far away from the reservoir. Changes in stress and strain happen mainly within the reservoir and they are not significant in other areas. Geomechanical modeling predicts significant changes in vertical displacements both in the reservoir and on ground even after a period of production. It remains to be determined what magnitude of change in seismic response will be produced by these complex competing processes.

## ACKNOWLEDGMENTS

We would like to express our appreciation to the CREWES sponsors for their support of this research. We also gratefully acknowledge Imperial Oil for their permission to use their seismic data.

## REFERENCES

- Kenter, C. J., Van den Beukel, A. C., Hatchell, P. J., Maron, K. P., Molenaar, M. M., 2004, Evaluation of reservoir characteristics from timeshifts in the overburden, American Rock Mechanics Association. ARMA/NARMS 04-627.
- Settari, Antonin and F. M. Mourits, 1998, A coupled reservoir and geomechanical simulation system, SPE Journal, 219-226.
- Settari, Antonin and Raisbeck, J. M., 1978, Fracture mechanics analysis in in-situ oil sands recovery. Paper 78-29-18, 29<sup>th</sup> Annual Technical Meeting of the Petroleum Society of the Canadian Institute of Mining and Metallurgy, Calgary, June 13-16, 1978.
- Walters, D. A. and A. Settari, 2000, Poreelastic effects of cyclic steam stimulation in the Cold Lake Reservoir, SPE 62590.
- Wang, Zhijing and A. Nur, 2000, Seismic and acoustic velocities in reservoir rocks, recent developments, Geophysics reprint series.

## NOTATIONS

$C_T$ : thermal conductivity (E/smT)  
g: gravity accelerator ( $m/s^2$ )  
 $H_f$ : enthalpy of fluid (E/kg)  
 $H_s$ : enthalpy of solid (E/kg)  
k: permeability ( $m^2$ )  
P: pressure ( $kg/m\ s^2$ )  
 $Q_f$ : source or sink of fluid (kg/s)  
 $Q_s$ : source or sink of solid (kg/s)  
 $Q_{heat}$ : source or sink of heat (E/s)  
S: total stress ( $kg/m\ s^2$ )  
T: temperature (T)  
t: time (t)  
 $U_f$ : internal energy of fluid (E/kg)  
 $U_s$ : internal energy of solid (E/kg)  
 $v_f$ : fluid velocity (m/s)  
 $v_s$ : solid velocity (m/s)  
 $\mu_f$ : viscosity of fluid (kg/sm)  
 $\rho_f$ : fluid density ( $kg/m^3$ )  
 $\rho_s$ : fluid density ( $kg/m^3$ )  
 $\phi$ : porosity  
E: energy  
kg: mass  
m: length  
s: time  
T: temperature  
V: volume